

Spin- and state-resolved charge transfer and excitation in low-energy He^{+}-Na(3s,3p) collisions

Xiao-Xia Wang(王小霞), Rui Tang(唐瑞), Li Ma(马丽), Chuan-Yu Zhang(张传瑜), Jian-Guo Wang(王建国), and Yi-Zhi Qu(屈一至)

Citation: Chin. Phys. B, 2026, 35 (**7**): 073402. DOI: 10.1088/1674-1056/ae705c
http://cpb.iphy.ac.cn; http://iopscience.iop.org/cpb

What follows is a list of articles you may be interested in

Charge transfer processes in low-energy Na^{+}-Na collisions

Cheng-Cheng Jiang(蒋承呈), Xiao-Xia Wang(王小霞), Kun Wang(王堃), Yi-Zhi Qu(屈一至), Jian-Guo Wang(王建国), Xia Li(李侠), Li Ma(马丽), and Robert J. Buenker

Chin. Phys. B, 2026, 35 (**4**): 043402. DOI: 10.1088/1674-1056/ae15f0

Single electron capture in low- and intermediate-energy collisions of $Si^{3,4+}$ with He

Yingzhou Li(李英卓), Yadong Liu(刘亚东), Yueying Qi(祁月盈), Ling Liu(刘玲), Yizhi Qu(屈一至), and Jianguo Wang(王建国)

Chin. Phys. B, 2026, 35 (**1**): 013401. DOI: 10.1088/1674-1056/ae15f4

Electron capture and excitation in intermediate-energy He^{2+}-H(1s,2s) collisions

Yadong Liu(刘亚东), Congcong Jia(贾聪聪), Mingxuan Ma(马茗萱), Xiang Gao(高翔), Ling Liu(刘玲), Yong Wu(吴勇), Xiangjun Chen(陈向军), and Jianguo Wang(王建国)

Chin. Phys. B, 2024, 33 (**8**): 083401. DOI: 10.1088/1674-1056/ad5322

Atomic structure and collision dynamics with highly charged ions

Xinwen Ma(马新文), Shaofeng Zhang(张少锋), Weiqiang Wen(汶伟强), Zhongkui Huang(黄忠魁), Zhimin Hu(胡智民), Dalong Guo(郭大龙), Junwen Gao(高俊文), Bennaceur Najjari, Shenyue Xu(许慎跃), Shuncheng Yan(闫顺成), Ke Yao(姚科), Ruitian Zhang(张瑞田), Yong Gao(高永), and Xiaolong Zhu(朱小龙)

Chin. Phys. B, 2022, 31 (**9**): 093401. DOI: 10.1088/1674-1056/ac8736

X-ray emission from 424-MeV/u C ions impacting on selected target

Xian-Ming Zhou(周贤明), Rui Cheng(程锐), Yu Lei(雷瑜), Yuan-Bo Sun(孙渊博), Yu-Yu Wang(王瑜玉), Xing Wang(王兴), Ge Xu(徐戈), Ce-Xiang Mei(梅策香), Xiao-An Zhang(张小安), Xi-Meng Chen(陈熙萌), Guo-Qing Xiao(肖国青), Yong-Tao Zhao(赵永涛)

Chin. Phys. B, 2016, 25 (**2**): 023402. DOI: 10.1088/1674-1056/25/2/023402

Spin- and state-resolved charge transfer and excitation in low-energy He^+–Na(3s,3p) collisions

Xiao-Xia Wang(王小霞)[1], Rui Tang(唐瑞)[1], Li Ma(马丽)[1], Chuan-Yu Zhang(张传瑜)[1], Jian-Guo Wang(王建国)[2], and Yi-Zhi Qu(屈一至)[3,†]

[1] *College of Physics, Chengdu University of Technology, Chengdu* 610059, *China*
[2] *Data Center for High Energy Density Physics, Institute of Applied Physics and Computational Mathematics, Beijing* 100088, *China*
[3] *College of Material Sciences and Optoelectronic Technology, University of Chinese Academy of Sciences, Beijing* 100049, *China*

(Received 20 March 2026; revised manuscript received 9 May 2026; accepted manuscript online 20 May 2026)

We present a theoretical study of charge-transfer (CT) and electron-excitation (EX) processes in collisions of He^+ with Na(3s) and Na(3p) using the quantum-mechanical molecular-orbital close-coupling (QMOCC) method. Adiabatic potential curves together with the corresponding radial and rotational nonadiabatic couplings are calculated for both singlet and triplet spin manifolds. State-resolved results show that, for He^+–Na(3s) collisions, the CT process is mainly governed by long-range Demkov-type interactions, with electron capture predominantly populating the He(1s2s) triplet state, while excitation cross sections are smaller and occur at shorter internuclear distances. In the He^+–Na(3p) system, additional Π-symmetry channels participate in the dynamics, leading to dominant capture into the He(1s2p) state. Despite the different initial electronic configurations, the total CT cross sections for Na(3p) are comparable in magnitude to those for Na(3s), with Σ-symmetry channels contributing more efficiently than Π channels. The calculated total CT cross sections for Na(3s) and Na(3p) are on the order of 10^{-18}–10^{-14} cm^2 and agree with the experimental data within deviations of about 5% and 10%–20% in the overlapping energy range. The present results show good agreement with available experimental and theoretical data, providing a comprehensive description of the state-resolved collision dynamics in the low- and intermediate-energy regimes.

Keywords: ion-atom collision, charge transfer, electron-excitation processes, quantum-mechanical molecular-orbital close-coupling (QMOCC) method

PACS: 34.70.+e, 34.20.−b

DOI: 10.1088/1674-1056/ae705c **CSTR:** 32038.14.CPB.ae705c

1. Introduction

Ion–atom collisions involving helium ions and alkali-metal atoms have long served as benchmark systems for investigating charge-transfer dynamics in atomic collision physics.[1–3] In particular, the He^+–Na system has attracted considerable interest due to its relatively simple electronic structure and well-defined molecular potential curves, which make it suitable for both experimental measurements and theoretical modeling.[4–6] Charge-transfer and excitation processes in such collisions play an important role in plasma physics, astrophysical environments, and laboratory ionized gases, where they influence charge-state distributions, energy transport, and spectral emissions.[1,7] Reliable cross sections for these processes are essential for plasma modeling and spectroscopic diagnostics.[8] Among the possible collision channels, the He^+ collisions with Na in the 3s and 3p states are of particular interest, since they represent typical ground-state and excited-state collision systems and provide valuable insight into the mechanisms of charge transfer and state-resolved population dynamics.[9]

Several experimental studies have been performed on the He^+–Na collision system, most of them focusing on electron transfer from the Na(3s) ground state. Absolute charge-transfer cross sections for He^+–Na(3s) collisions have been investigated using ion-beam vapor/gas-target and crossed-beam techniques with charge-state analysis, spanning studies by Nagata *et al.*[10] (0.4–5 keV), DuBois and Toburen[11] (2–100 keV), and Aumayr *et al.*[12] (2–20 keV). For the excited Na(3p) state, Houver *et al.*[13] investigated charge-transfer processes in the 0.5–3 keV range using time-of-flight spectroscopy, while Thomsen *et al.*[14] extended the measurements to the 1–15 keV range using a crossed-beam setup combined with laser optical pumping and time-of-flight spectroscopy. Their measurements mainly provided ratios of capture cross sections from Na(3p) relative to Na(3s), which can be combined with the available absolute data for Na(3s) to estimate capture cross sections from the excited states.

On the theoretical side, electron transfer from the Na(3s) ground state has been investigated using a variety of models, including the one-electron molecular description of Sidis *et al.*,[4] the one-electron atomic-basis model of Rod and Nielsen,[9,15] the two-electron molecular approach of Mó

†Corresponding author. E-mail: yzqu@ucas.ac.cn

© 2026 Chinese Physical Society and IOP Publishing Ltd. All rights, including for text and data mining, AI training, and similar technologies, are reserved.

and Riera,[5] and the close-coupling treatment with two-electron molecular- and atomic-orbital expansions developed by Fritsch *et al.*[6] Although these calculations show reasonable agreement with experimental data in overall magnitude, discrepancies remain in the detailed energy dependence of the cross sections. For collisions involving the Na(3p) excited state, the one-electron atomic-basis model of Rod and Nielsen,[9,15] and two-electron molecular calculations were reported by Mó and Riera[16] and later by Dutta *et al.*,[17] where the capture channels were mainly limited to the He(1s2s) and He(1s2p) singlet and triplet states. In addition, measurements of orbital-alignment effects by Thomsen *et al.*[14] revealed significant differences between the experimental and theoretical cross-section ratios, suggesting that a more complete theoretical description of the collision dynamics is still needed.

In the present work, we perform a systematic theoretical investigation of collisions between He^+ ions and Na atoms in the 3s and 3p initial states using the full quantum-mechanical molecular-orbital close-coupling (QMOCC) method.[18–20] The following charge-transfer (CT) and electron-excitation (EX) processes are considered:

$$\begin{aligned} \mathrm{He}^+(1s)+\mathrm{Na}(2p^6 3s) &\rightarrow \mathrm{He}(1s2l^{1,3}\mathrm{L})+\mathrm{Na}^+(2p^6) \quad (\mathrm{CT}) \\ &\rightarrow \mathrm{He}^+(1s)+\mathrm{Na}(2p^6 3p/4s) \quad (\mathrm{EX}), \end{aligned} \tag{1}$$

$$\mathrm{He}^+(1s)+\mathrm{Na}(2p^6 3p) \rightarrow \mathrm{He}(1s2l^{1,3}\mathrm{L})+\mathrm{Na}^+(2p^6) \quad (\mathrm{CT}). \tag{2}$$

Adiabatic potential energy curves, together with the corresponding nonadiabatic radial and rotational coupling matrix elements, are calculated for both singlet and triplet spin manifolds using the multireference single- and double-excitation configuration interaction (MRD-CI) method.[21–23] Based on these quantities, total and state-resolved cross sections for charge transfer and electron excitation are obtained over a wide range of collision energies. Special attention is paid to the role of molecular symmetry and long-range interactions in determining the dominant transition channels. The calculated results are compared with available experimental measurements and previous theoretical studies to elucidate the underlying collision mechanisms and to provide reliable cross-section data for the He^+–Na system. The present study provides a comprehensive and consistent dataset for both ground and excited initial states, which is essential for plasma modeling and astrophysical applications.

2. Theoretical methods

2.1. $HeNa^+$ molecular ion

The electronic structure of the $HeNa^+$ system was computed over an internuclear distance range of 1.0–50.0 a.u. using the *ab initio* MRD-CI quantum chemistry package.[24] For He, the aug-cc-pVQZ (augmented correlation consistent polarization valence quadruple ζ) basis[25] was employed, i.e., (8s,4p,3d) contracted to [5s,4p,3d]. The f and g Gaussian-type functions were omitted, as they have negligible impact on the accuracy of the electronic structure. To accurately describe the Rydberg states of He, a diffuse (1s, 1p, 1d) basis set was additionally included. For Na, the 1s electrons were treated with the CRENBL effective core potential,[26] while the remaining electrons were described using a [6s, 4p] basis set augmented by diffuse (3s, 2p, 2d) functions. The Na 2s orbital was frozen, leaving eight active electrons for the MRD-CI calculations.

For the $HeNa^+$ system, six $^1\Sigma^+$ (five $^3\Sigma^+$) states in A_1 symmetry and two $^1\Pi$ (two $^3\Pi$) states of B_1 symmetry, corresponding to the charge-transfer and excitation channels, were included in the singlet and triplet manifolds. Tables 1 and 2 list the asymptotic energy levels of the $HeNa^+$ atomic states for the singlet and triplet manifolds, compared with the experimental atomic energies from NIST.[27] For clarity, all energies are referenced to the entrance channel $He^+ + Na(3s)$, which corresponds to the second singlet state ($2^1\Sigma^+$) in Table 1 and the first triplet state ($1^3\Sigma^+$) in Table 2; these reference states are set to zero energy. The $2^1\Sigma^+/1^3\Sigma^+$ and $5^1\Sigma^+/4^3\Sigma^+$, as well as $2^1\Pi/2^3\Pi$ states (shown in boldface) asymptotically corresponding to the $He^+ + Na(3s)$ and $He^+ + Na(3p)$ atomic states, denote the initial collision channels, respectively. The differences between our calculated energies and the experimental values[27] are below 0.07 eV in the asymptotic region, which is sufficiently accurate for the subsequent scattering calculations.[28]

Table 1. Asymptotic atomic energies for the $HeNa^+$ molecular states to the singlet states.

Molecular states	Asymptotic atomic states	Energy (eV)		
		NIST	MRDCI	Error
$1^1\Sigma^+$	$He(1s^2\ ^1S)+Na^+(2s^22p^6\ ^1S)$	−19.448	−19.518	−0.07
$\mathbf{2^1\Sigma^+}$	$\mathbf{He^+(1s2s\ ^1S)+Na(2p^63s\ ^2S)}$	**0**	**0**	**0**
$3^1\Sigma^+$	$He(1s2s\ ^1S)+Na^+(2s^22p^6\ ^1S)$	1.167	1.096	−0.071
$4^1\Sigma^+,1^1\Pi$	$He(1s2p\ ^1P^\circ)+Na^+(2s^22p^6\ ^1S)$	1.770	1.716	−0.054
$\mathbf{5^1\Sigma^+,2^1\Pi}$	$\mathbf{He^+(1s\ ^2S)+Na(2p^63p\ ^2P^\circ)}$	**2.102**	**2.067**	**−0.035**
$6^1\Sigma^+$	$He^+(1s\ ^2S)+Na(2p^64s\ ^2S)$	3.191	3.174	−0.017

Table 2. Asymptotic atomic energies for the $HeNa^+$ molecular states to the triplet states.

Molecular states	Asymptotic atomic states	Energy (eV)		
		NIST	MRDCI	Error
$1^3\mathbf{\Sigma}^+$	$He^+(1s\ ^2S)+Na(2p^63s\ ^2S)$	**0**	**0**	**0**
$2^3\Sigma^+$	$He(1s2s\ ^3S)+Na^+(2s^22p^6\ ^1S)$	0.371	0.352	−0.19
$3^3\Sigma^+,1^3\Pi$	$He(1s2p\ ^3P^\circ)+Na^+(2s^22p^6\ ^1S)$	1.516	1.474	−0.042
$4^3\mathbf{\Sigma}^+,2^3\mathbf{\Pi}$	$\mathbf{He^+(1s\ ^2S)+Na(2p^63p\ ^2P^\circ)}$	**2.102**	**2.071**	**−0.031**
$5^3\Sigma^+$	$He^+(1s\ ^2S)+Na(2p^64s\ ^2S)$	3.191	3.173	−0.018

2.2. Scattering calculations

Nonradiative charge-transfer and excitation cross sections are calculated using the QMOCC method.[18–20] Within the perturbed stationary state (PSS) model,[3,20,29] the total wave function is expanded in terms of adiabatic electronic states. After performing a partial-wave expansion for each channel, the radial functions $f^J(R)$ satisfy a set of coupled differential equations in the rotating coordinate system:

$$\left[\frac{\mathrm{d}^2}{\mathrm{d}R^2}-\frac{J(J+1)-\lambda^2}{R^2}-2\mu(u(R)-E)\right]f^J(R) = (V^R(R)+V^C(R))f^J(R), \tag{3}$$

where μ is the reduced mass and u is the diagonal adiabatic potential matrix. The quantities $J(J+1)$ and λ are the eigenvalues of the total angular momentum and the projection of the electronic angular momentum, respectively. V^R and V^C represent the radial and rotational coupling matrices, which are defined as

$$V^R_{ij}(R) = \left[\langle i|-\frac{\partial^2}{\partial R^2}+\frac{L_x^2+L_y^2}{R^2}|j\rangle-2\langle i|\frac{\partial}{\partial R}|j\rangle\frac{\partial}{\partial R}\right]\delta_{\lambda_i,\lambda_j}, \tag{4a}$$

$$V^C_{ij}(R) = -2\delta_{\lambda_i,\lambda_j+1}\left[(J-\lambda_i)(J+\lambda_i+1)\right]^{1/2}\frac{\langle i|\,\mathrm{i}L_y\,|j\rangle}{R^2} +2\delta_{\lambda_i,\lambda_j-1}\left[(J+\lambda_i)(J-\lambda_i+1)\right]^{1/2}\frac{\langle i|\,\mathrm{i}L_y\,|j\rangle}{R^2}. \tag{4b}$$

The radial coupling elements, typically evaluated by finite-difference methods, may vary rapidly near avoided crossings. To obtain smoother couplings, a unitary transformation from the adiabatic to the diabatic representation is introduced. This transformation yields a diabatic potential matrix $U(R)$, whose off-diagonal elements govern the charge-transfer process. Accordingly, the radial functions are transformed, and the coupled equations take the form

$$\left[\frac{\mathrm{d}^2}{\mathrm{d}R^2}-\frac{J(J+1)-\lambda^2}{R^2}+2\mu E\right]g^J_\gamma-2\mu\sum_{\gamma'}U_{\gamma,\gamma'}(R)g^J_{\gamma'}=0. \tag{5}$$

When $R\to\infty$, the internuclear interaction can be neglected. Therefore, the radial coupled equations satisfy the asymptotic boundary conditions

$$g^J_i(R)\xrightarrow[R\to\infty]{}\frac{1}{\sqrt{k_j}}[\delta_{ij}j_J(k_iR)+K^J_{ij}\eta_J(k_jR)], \tag{6}$$

where $k_i^2=2\mu[E-\varepsilon_i(\infty)]$, j_J and η_J denote the regular and irregular Riccati–Bessel functions for neutral channels, or the regular and irregular Coulomb functions[30] for ionic channels, respectively. In the present calculations, the value of $R_{\max}$ for matching the boundary conditions is taken from 10000 a.u. to 500 a.u. For $R>50$ a.u. the interaction potentials are smoothly extended using the dipole polarization form $V_{\mathrm{pol}}(R)=-\frac{\alpha_{\mathrm{d}}q^2}{2R^4}$, where α_{d} is the dipole polarizability of the neutral atom (He or Na), and q is the charge of the ionic core (He^+ or Na^+).[31] The coupled-channel equations are solved using the Johnson log-derivative method.[32] By matching the asymptotic boundary conditions, the K^J matrix is obtained, and the corresponding scattering matrix is given by

$$S^J=\frac{I+\mathrm{i}K^J}{I-\mathrm{i}K^J}. \tag{7}$$

Finally, the integral cross section for a transition from channel i to j is calculated from the scattering matrix elements as

$$\sigma_{(i\to j)}=\frac{\pi}{k_i^2}\sum_J(2J+1)\left|\delta_{ij}-S^J_{ij}\right|^2, \tag{8}$$

where k_i is the initial momentum in center-of-mass frame and δ_{ij} is the Kronecker delta. The quantum number J denotes the partial-wave angular momentum, and convergence with respect to the partial-wave expansion is achieved by increasing $J_{\max}$ until the cross sections change by less than 10^{-10} a.u. At intermediate energies, the electron translation factors (ETF) are included to correct the boundary conditions. Following the scheme of Gargaud,[3,33] the radial and rotational couplings are modified accordingly to account for translation effects.

3. Adiabatic potentials and couplings

With the exception of the lowest singlet state $[He(1s^2)+Na^+(2s^22p^6);1^1\Sigma^+]$, all Σ^+ and Π states included in the present singlet and triplet manifolds are shown in Figs. 1(a) and 1(b) for internuclear distances $R=1.0$–30.0 a.u. The electronic structures obtained with the present MRD-CI method are compared with the configuration-interaction (CI) results of Dutta *et al.*,[17] in which the $HeNa^+$ system was treated as a quasi-two-electron system using a Gaussian-type pseudopotential. Taking the $[He^+ + Na(3p);5^1\Sigma^+]$ state as the

reference, the potential energy curves show generally good agreement in shape. However, the $[He^+ + Na(3p); 4^3\Sigma^+]$ and $[He^+ + Na(3s)/Na(4s)]$ asymptotic states in Dutta *et al.*[17] are lower than the present results by about 0.20 eV and 0.27 eV, respectively, in the asymptotic region. These differences are mainly attributed to the different CI treatments and the corresponding descriptions of electron–correlation effects in the two calculations. The omitted lowest singlet state lies about 19.5 eV below the nearest channel and is therefore expected to contribute negligibly to the charge-transfer dynamics. Since the collision partners are singly charged, the long-range interaction is dominated by polarization, leading to rather smooth potential curves. As a consequence, no pronounced avoided crossings are observed for $R > 8.0$ a.u. in either manifold, indicating that low-energy charge transfer is not controlled by localized Landau–Zener-type transitions at well-defined crossing points.[3]

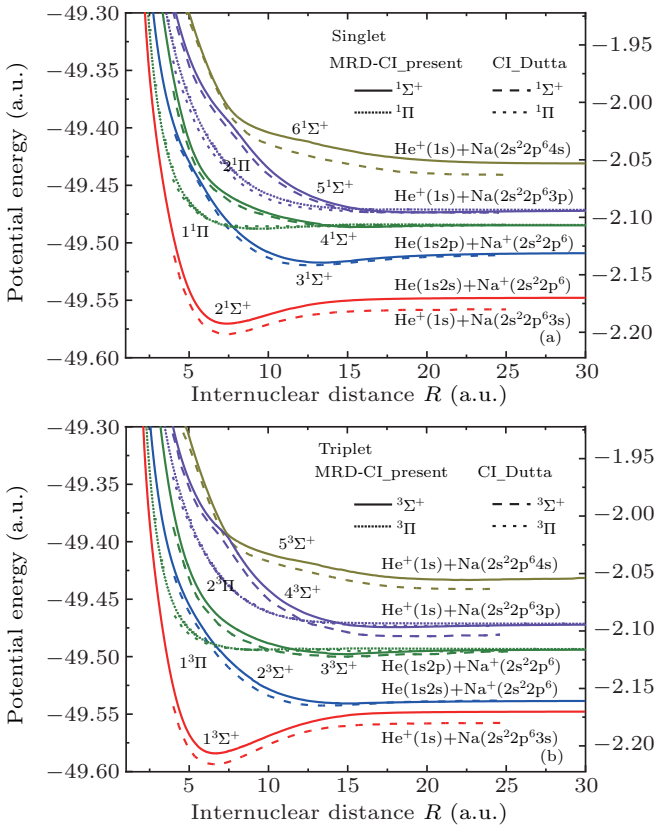


Fig. 1. Adiabatic potential curves of $HeNa^+$ molecular states from the present MRD-CI method and CI of Dutta *et al.*[17] in the singlet (a) and triplet (b) spin manifolds.

Charge-transfer channels $[He(1s2s) + Na^+; 3^1\Sigma^+/2^3\Sigma^+]$ and $[He(1s2p) + Na^+; 4^1\Sigma^+/3^3\Sigma^+]$ are the closest in energy to the entrance channels $[He^+ + Na(3s); 2^1\Sigma^+/1^3\Sigma^+]$ and $[He^+ + Na(3p); 5^1\Sigma^+/4^3\Sigma^+]$, respectively, and are therefore expected to constitute the dominant exit channels for charge transfer. In this situation, the dynamics can be interpreted within a Demkov-type mechanism,[31,34] in which the transition probability at low energies is largely governed by the asymptotic energy defect between the entrance and exit channels. Compared with the singlet manifold, the energy separation between $[He(1s2s) + Na^+]$ and $[He^+ + Na(3s)]$ is smaller in the triplet manifold, suggesting that charge transfer in He^+–Na(3s) collisions is dominated by triplet transitions. In contrast, for He^+–Na(3p) collisions, the corresponding singlet energy defect is smaller, implying that singlet charge transfer provides the main contribution.

Pronounced avoided crossings appear only at shorter distances. In particular, crossings occur between $[He(1s2s) + Na^+; 3^1\Sigma^+/2^3\Sigma^+]$ and $[He(1s2p) + Na^+; 4^1\Sigma^+/3^3\Sigma^+]$ near $R \approx 5.6$ a.u., as well as between $[He^+ + Na(3p); 5^1\Sigma^+/4^3\Sigma^+]$ and $[He^+ + Na(4s); 6^1\Sigma^+/5^3\Sigma^+]$ around $R \approx 7.5$ a.u. These short-range interactions are expected to become increasingly important at higher collision energies, where smaller internuclear separations are more effectively sampled.

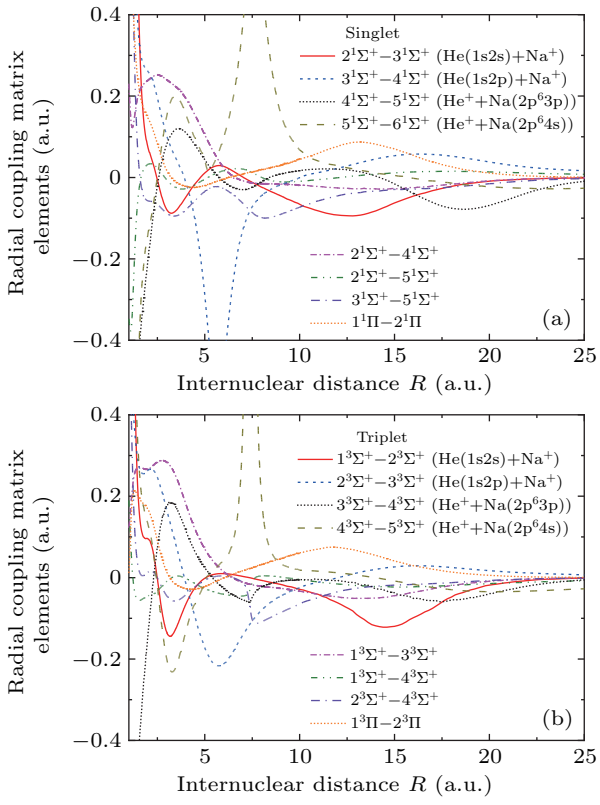


Fig. 2. Radial coupling matrix elements of $HeNa^+$ molecular states as a function of internuclear distance: (a) singlet states; (b) triplet states.

These avoided crossings are accompanied by strong radial couplings, as shown in Fig. 2. As can be seen from Fig. 2, apart from the pronounced interactions between $[He(1s2s) + Na^+; 3^1\Sigma^+/2^3\Sigma^+]$ and $[He(1s2p) + Na^+; 4^1\Sigma^+/3^3\Sigma^+]$, as well as between $[He^+ + Na(3p); 5^1\Sigma^+/4^3\Sigma^+]$ and $[He^+ + Na(4s); 6^1\Sigma^+/5^3\Sigma^+]$ around 5.6 a.u. and 7.5 a.u., respectively, the radial couplings among the low-lying states remain relatively weak. Most coupling matrix elements exhibit broad and shallow long-range structures rather than sharp localized

peaks. Such coupling profiles are characteristic of Demkov-type interactions, which typically dominate low-energy charge transfer when the entrance and exit channels are near but do not form strong avoided crossings at large R. Consistent with the potential-curve analysis, the $3^1\Sigma^+/2^3\Sigma^+$ and $4^1\Sigma^+/3^3\Sigma^+$ states are the closest exit channels to the entrance channels $2^1\Sigma^+/1^3\Sigma^+$ and $5^1\Sigma^+/4^3\Sigma^+$, respectively. Accordingly, broad long-range maxima appear in the corresponding radial couplings around 13 a.u. and 17 a.u. Similar long-range features are also observed in the Π states, e.g., between $1^1\Pi/1^3\Pi$ and $2^1\Pi/2^3\Pi$ near 12 a.u. These long-range couplings therefore constitute the primary gateway for charge-transfer flux from the entrance channels to the dominant exit channels, and are expected to provide the major contribution to the total charge-transfer cross sections at low collision energies.

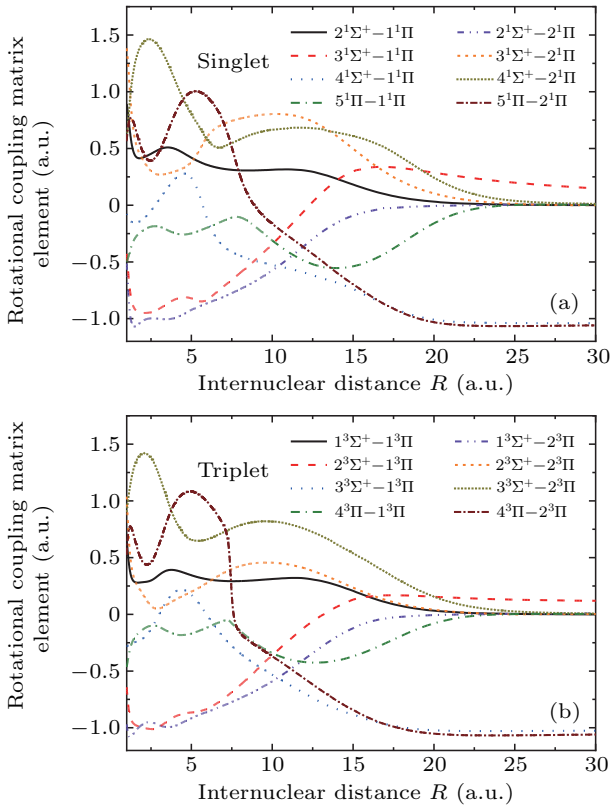


Fig. 3. Rotational coupling matrix elements of $HeNa^+$ molecular states as a function of internuclear distance: (a) singlet states; (b) triplet states.

Electrons can also be transferred to states of different symmetries through rotational couplings. As shown in Fig. 3, the rotational coupling matrix elements in the singlet manifold are formally similar to those in the triplet manifold. For $R < 20$ a.u., the Σ–Π couplings involving the entrance channels $2^1\Sigma^+/1^3\Sigma^+$ and $5^1\Sigma^+/4^3\Sigma^+$ exhibit broad, slowly varying long-range structures, which are characteristic of Demkov-type interactions. In the short-range region, several Σ–Π couplings become markedly enhanced, implying that Π-state population may also be promoted at higher impact energies. Notably, the largest Σ–Π couplings are mainly associated with channels correlated to the $He(1s2p)+Na^+$ and $He^+ + Na(3p)$ asymptotes, indicating that Π channels provide additional pathways for both charge-transfer and excitation processes. Consequently, although the dominant charge-transfer flux is governed by same-symmetry transitions driven by radial couplings, rotational couplings can still contribute appreciably to electron transfer into states of different symmetries.

4. Collisions of He^+ with Na(3s)

4.1. Total charge-transfer cross sections

Based on the electronic-structure analysis of the $HeNa^+$ quasimolecule, the CT cross sections for the singlet and triplet manifolds are calculated using the QMOCC method over the impact-energy range of 0.002–7 keV/amu. The total CT cross sections, obtained by spin-averaging the singlet (25%) and triplet (75%) contributions, are shown in Fig. 4.

Below 380 eV/amu, the present QMOCC results are slightly higher than other theoretical predictions, while remaining in reasonable agreement with the measurements of Nagata *et al.*[10] with the difference being less than 5%. Starting from collision energies around 90 eV/amu, the one-electron MO model of Sidis *et al.*[4] begins to yield smaller cross sections than the present QMOCC results. This discrepancy can be attributed to the simplified one-electron description adopted in that model, which may not fully capture the detailed molecular features and multichannel couplings of the $HeNa^+$ collision system. In the low-energy region, the charge-transfer process is mainly governed by long-range quasi-resonant interactions between the entrance channel $He^+(1s)+Na(3s)$ and the exit channels $He(1s2l)+Na^+$, making the transition probabilities particularly sensitive to the accuracy of the molecular potentials and nonadiabatic couplings.

In the energy range of 380 eV/amu–2 keV/amu, the present results agree well with the atomic-orbital (AO) calculations of Fritsch *et al.*[6] and the molecular-orbital (MO) results of Mó *et al.*[5] and lie between the experimental measurements of DuBois *et al.*[11] and Aumayr *et al.*[12] This overall consistency indicates that the dominant nonadiabatic couplings are adequately described within the present QMOCC framework. A discrepancy of about 20% is observed between the present cross sections and those obtained from the semiclassical molecular-orbital close-coupling (MOCC) calculations of Fritsch *et al.*[6] This difference can be attributed to the distinct theoretical approaches employed. The collision dynamics of Fritsch *et al.*[6] were treated within the semiclassical MOCC framework, where the nuclear motion is described classically, making it more suitable for intermediate- and high-energy collisions. In contrast, the present QMOCC

method provides a fully quantum-mechanical description and is therefore more appropriate for low-energy processes, where nonadiabatic couplings and quantum interference effects play a significant role.

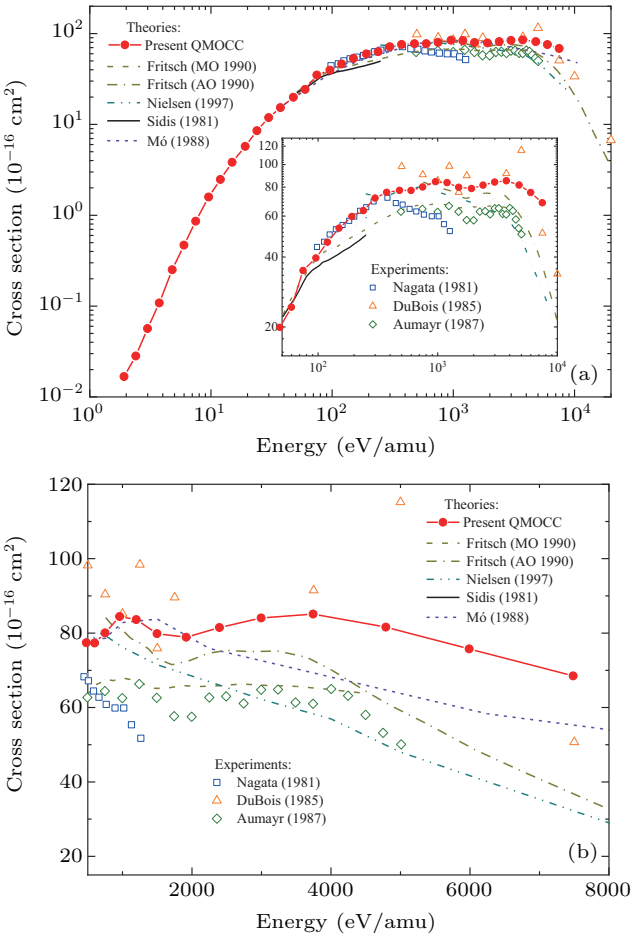


Fig. 4. Spin-averaged total charge-transfer cross sections for He^+–Na(3s) collisions: (a) logarithmic scale; (b) linear scale from 500–8000 eV/amu. Theory: present QMOCC (solid line with filled circles), Sidis *et al.*[4] (solid line), Mó *et al.*[5] (dashed line), Fritsch *et al.*[6] (dash-dotted line), Nielsen *et al.*[9] (dash-dot-dot line). Experiment: Aumayr *et al.*[12] (open diamonds), DuBois *et al.*[11] (open triangles), Nagata *et al.*[10] (open squares).

In addition, a weak oscillatory structure is observed from 380 eV/amu to 7 keV/amu, with a shallow minimum near 1.8 keV/amu. Similar features can also be identified in the experimental data of Aumayr *et al.*[12] and in the AO calculations of Fritsch *et al.*[6] These oscillations are generally attributed to Stueckelberg-type[35] interference arising from coherent transitions at successive avoided crossings along the collision path. The phase difference accumulated between different transition pathways, which depends on the energy gap between the interacting molecular potentials and the collision velocity, may lead to constructive or destructive interference, resulting in the observed modulations in the cross sections. Although the QMOCC results are significantly higher than previous works in the 2–7 keV/amu range, we include the data in this range to better illustrate the oscillatory structure.

4.2. Total electron-excitation cross sections

The total spin-averaged excitation cross sections are obtained by summing over all transitions from the entrance channel to the excited Na(3p/4s) states. The contributions from singlet and triplet manifolds are combined using statistical weights of 1/4 and 3/4, respectively. The resulting spin-averaged excitation cross sections for the $He^+ + Na(3s)$ system are presented in Fig. 5. Compared with the charge-transfer channel, the excitation cross sections are systematically smaller over the entire collision energy range, which can be attributed to the larger energy separations between the entrance channel and the excited Na states, leading to reduced nonadiabatic transition probabilities. From a dynamical point of view, excitation processes predominantly occur at shorter internuclear distances than charge-transfer processes. In this region, the electronic structure of the collision complex is more strongly perturbed, resulting in enhanced multichannel couplings and more complex interaction patterns. Consequently, the excitation cross sections are particularly sensitive to the accuracy of the molecular potential energy curves and the coupling matrix elements.

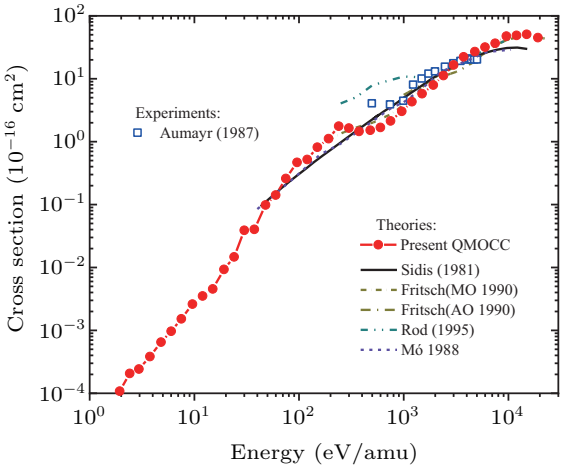


Fig. 5. Spin-averaged electron excitation cross sections of Na(3s) and comparison with other results. Theory: present QMOCC (solid line with filled circles), Sidis *et al.*[4] (solid line), Mó *et al.*[5] (dashed line), Fritsch *et al.*[6] (dash-dotted line), Rod *et al.*[9,15] (dash-dot-dot line). Experiment: Aumayr *et al.*[12] (open squares).

The available experimental data of Aumayr *et al.*[12] exhibit an overall energy dependence consistent with the present QMOCC calculations. Notably, a plateau is observed near 600 eV/amu in our results, in agreement with the experimental trend. This feature may be associated with the balance between increasing nonadiabatic transition probabilities and the decreasing interaction time at intermediate collision energies. The slightly higher cross sections reported by Aumayr *et al.*[12] can be attributed to cascading contributions from higher excited states, which may enhance the apparent excitation yields. Theoretical results of Mó *et al.*[5] and Fritsch *et al.*[6] based on the MO approach also show reasonable agreement,

with minor differences in magnitude, likely due to variations in basis sets or the treatment of electron translation factors among the different calculations. The overestimation reported by Rod *et al.*[9,15] in the energy range of 250–1300 eV/amu is likely related to the simplified one-electron description employed in their model.

4.3. State-resolved cross sections

The total CT cross section from the Na(3s) initial state exhibits a clear energy dependence. With increasing collision energy, the CT cross section changes from a rapidly varying behavior at low energies to a gradually saturating trend at higher energies. To investigate the CT process in more detail, the state-resolved cross sections for electron capture into He(1s2l) and Na(3p/4s) are presented in Figs. 6 and 7 and compared with the theoretical AOCC results of Nielsen *et al.*[9] and the MO calculations of Mó *et al.*[5] The present results are generally consistent with the available data in the overlapping energy range. At collision energies below 250 eV/amu, the larger He(1s2p) cross sections reported by Mó *et al.*[5] likely arise from their use of a semiclassical impact parameter formalism, in which the electronic wavefunction of the colliding system is expanded over a twelve-state molecular basis. This approach is less accurate than the present QMOCC method at low energies.

In the low-energy region, the CT process is primarily governed by exit channels such as He(1s2s) and He(1s2p), which are close in energy to the entrance channel. The transitions in this regime exhibit typical characteristics of the Demkov-type mechanism arising from long-range interactions. For capture into the He(1s2s), the He(1s2s) ($2^3\Sigma^+$) triplet state is strongly favored over the corresponding singlet states. This behavior can be understood in terms of both the smaller energy defect and the stronger coupling in the triplet manifold. As shown in Fig. 1, the energy separation between the entrance channel $[\mathrm{He}^+ + \mathrm{Na}(3s); 1^3\Sigma^+]$ and the nearest exit channel $[\mathrm{He}(1s2s) + \mathrm{Na}^+; 2^3\Sigma^+]$ is significantly smaller than that for the corresponding singlet channels at large internuclear distances. At the same time, Fig. 2 indicates that the associated radial coupling is slightly stronger for the triplet states in the same region. The combined effect of a smaller energy defect and enhanced coupling leads to a higher transition probability and, consequently, a larger cross section for the triplet channel.

By summing the state-resolved cross sections for electron capture into He($1s2l$), the total CT cross sections for He($n = 2$) in singlet and triplet manifolds are obtained. Figure 7 presents the cross sections for charge transfer to He($n = 2$) in panel (a) and for excitation to Na(3p/4s) in panel (b) for both singlet (S) and triplet (T) states. In Fig. 7(a), the capture cross sections into the He($n = 2$) states obtained from the present QMOCC calculations are compared with the available AOCC results of Nielsen *et al.*[9] and Fritsch *et al.*,[6] as well as the MO calculations of Mó *et al.*[5] Overall, the present results show good agreement with previous theoretical data in the overlapping energy range, although some deviations appear at intermediate energies. These differences may be related to the different dynamical treatments and basis sets adopted in the various calculations.

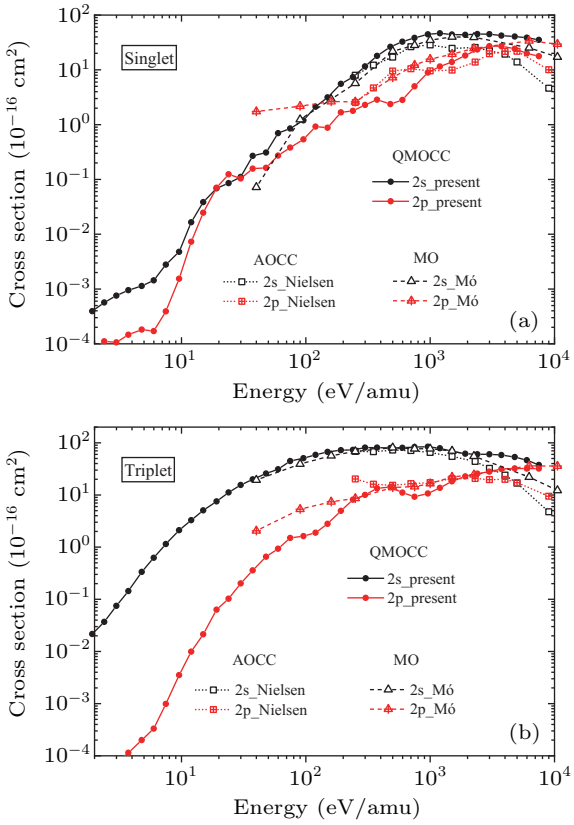


Fig. 6. State-resolved cross sections for charge transfer to He(1s2l) in He^+–Na(3s) collisions, compared with the results of Mó *et al.*[5] and Nielsen *et al.*[9] for (a) singlet state and (b) triplet state.

Figure 7(b) shows the state-resolved cross sections for electron excitation to the Na(3p) and Na(4s) states. In the low-energy region, the Na(3p) channel dominates the excitation process due to its smaller energy defect relative to the entrance channel. As the collision energy increases, the contribution of the Na(4s) channel becomes more significant. The present QMOCC results are generally lower than the AOCC data reported by Nielsen *et al.*[9] This difference may arise from the different theoretical approximations adopted in the two methods. In the AOCC model, the collision system is treated within a one-electron framework where the active electron moves in an effective potential, while multielectron correlations and some detailed molecular couplings are only approximately described. These approximations may influence the predicted transition probabilities.

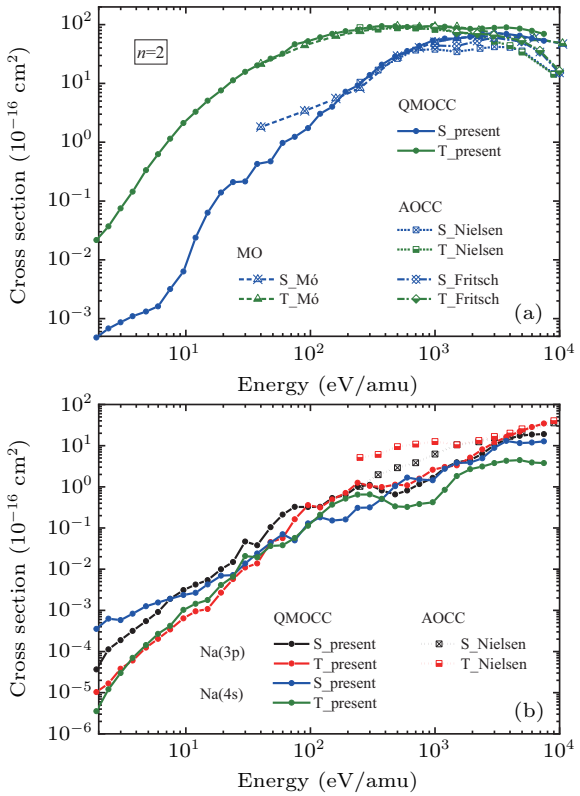


Fig. 7. State-resolved cross sections for charge transfer to He($n = 2$) in panel (a) and for excitation to Na(3p) and Na(4s) in panel (b) in the singlet (S) and triplet (T) states of He^+–Na(3s) collisions, compared with the results of Mó *et al.*,[5] Nielsen *et al.*[9] and Fritsch *et al.*[6]

5. Collisions of He^+ with Na(3p)

5.1. Total charge-transfer cross sections

Figure 8 presents the total charge-transfer (CT) cross sections for the He^++ Na(3p) collision system obtained with the present QMOCC calculations. The results are compared with available theoretical and experimental data in the impact-energy range of 0.002–7 keV/amu. Compared with the ground-state collision system He^++ Na(3s), the electron-capture mechanism for Na(3p) is more complicated because several molecular symmetries are involved. The entrance channels correspond to the $5^1\Sigma^+$, $2^1\Pi$, $4^1\Sigma^+$ and $2^3\Pi$ molecular states. To compare with experimental results, the total charge-transfer cross section is obtained by statistically averaging over all contributing channels. The statistical weight of the singlet and triplet manifolds is taken as 1:3, while the relative weights of the Σ and Π symmetries are assumed to be 1:2. The final cross section is therefore calculated as the weighted sum of the corresponding state-resolved cross sections.

Overall, the calculated cross sections exhibit a similar magnitude and energy dependence to previous theoretical predictions and experimental measurements. At collision energies below 750 eV/amu, the present QMOCC results are slightly lower than other theoretical predictions. In the intermediate energy range of 0.75–4 keV/amu, the present QMOCC results lie between the one-electron model calculations of Nielsen *et al.*[9] and the semiclassical impact-parameter approach based on a molecular-orbital expansion (IPMO) of Dutta *et al.*[17] At collision energies above 4 keV/amu, the present results become somewhat larger than those reported by Nielsen *et al.*[9] This discrepancy can be mainly attributed to the fact that the number of channels considered in the calculations is not sufficient. As described by Houver *et al.*,[13] "the He($n = 2$) and He($n = 3$) channels are populated: the He($n = 2$) reaction is dominant at low energies whereas the He($n = 3$) reaction becomes important at higher energies and/or scattering angles." In the energy range of 0.16–3.75 keV/amu, the total CT cross sections for Na(3p) are found to agree with the experimental data of Houver *et al.*[13] and Thomsen *et al.*[14] within a deviation of 10%–20%.

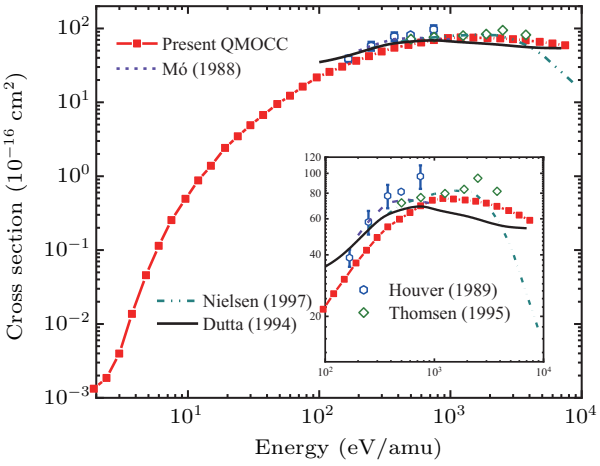


Fig. 8. Spin-average total charge transfer cross sections in He^+Na(3p) collisions. Theory: present QMOCC (solid line with filled square), Dutta *et al.*[17] (solid line), Mó *et al.*[16] (dashed line), Nielsen *et al.*[9] (dash-dot-dot line). Experiment: Thomsen *et al.*[14] (full diamond), Houver *et al.*[13] (open hexagon).

5.2. State-resolved cross sections

The state-resolved cross sections for electron capture to the He(1s2l) states are displayed in Fig. 9 for the different initial molecular states $5^1\Sigma^+$, $2^1\Pi$, $4^3\Sigma^+$ and $2^3\Pi$. The present QMOCC results are compared with the theoretical predictions obtained using the semiclassical impact-parameter molecular-orbital (IPMO) method reported by Dutta *et al.*[17] To clarify the origin of the differences between the two calculations, we performed additional test calculations using essentially the same eight molecular states adopted in Dutta *et al.*[17] The results indicate that the contributions from the $3^1\Pi$ and $3^3\Pi$ states are negligible, suggesting that the discrepancies do not mainly arise from the number of coupled channels included in the calculations.

In addition to the comparison of the potential energy curves shown in Fig. 1, the available coupling matrix elements reported by Dutta *et al.*[17] are compared with the present re-

sults in Fig. 10. Although the coupling matrix elements obtained in the two calculations exhibit generally similar profiles, noticeable differences remain in their magnitudes and spatial distributions over the broad interaction region. Since the electron-capture dynamics is highly sensitive to the strength and localization of the couplings, such differences may lead to appreciable variations in the state-resolved cross sections.

Moreover, only a limited number of coupling matrix elements were reported in Dutta *et al.*[17] and several important interactions cannot be directly compared, particularly the $4^1\Sigma^+$–$5^1\Sigma^+$ and $1^3\Pi$–$2^3\Pi$ couplings, which play significant roles in the nonadiabatic transition dynamics. In addition, the IPMO approach treats the nuclear motion semiclassically, whereas the present QMOCC method solves the coupled-channel equations fully within a quantum-mechanical framework. The quantum treatment is expected to provide a more consistent description of multichannel interference and nonadiabatic transition processes in the low- and intermediate-energy regions.

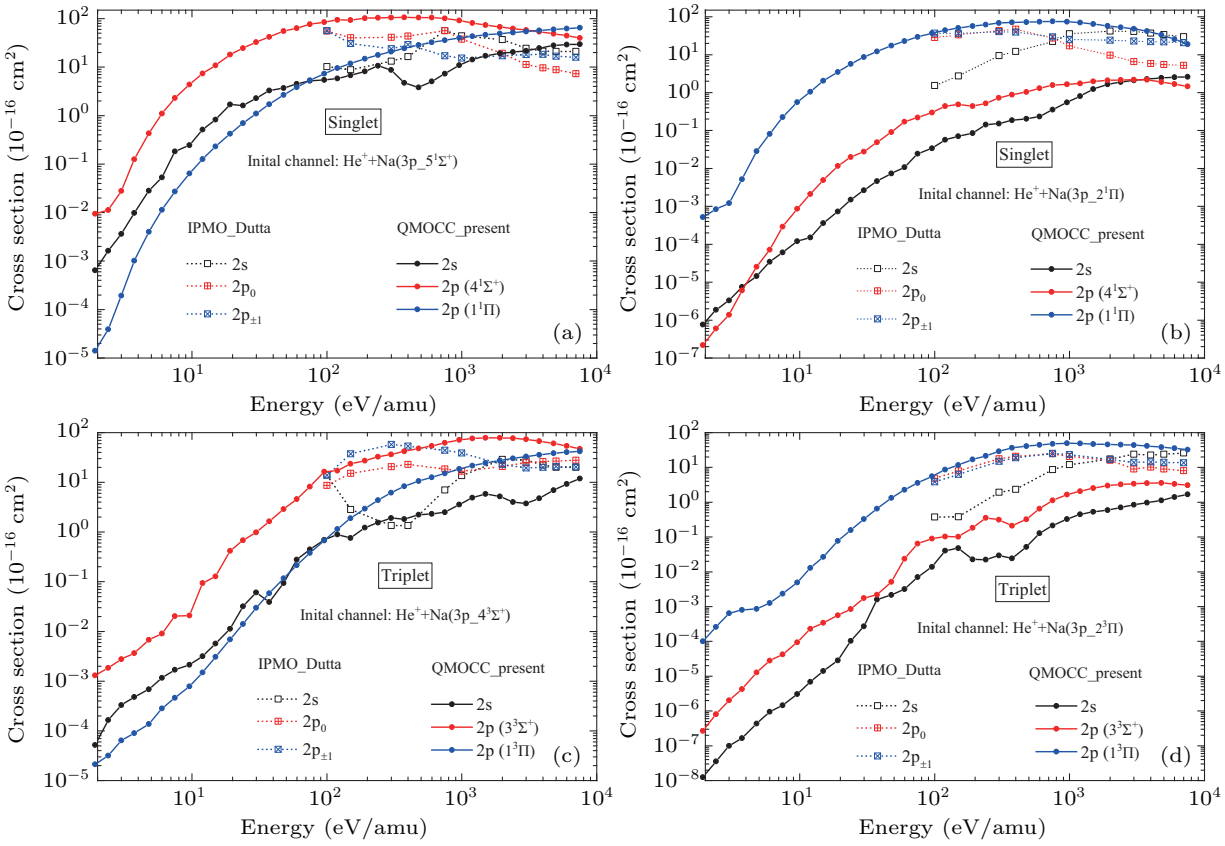


Fig. 9. State-resolved cross sections for charge transfer to He (1s2l) in He^+–Na(3p) collisions from different initial states, compared with the IPMO results of Dutta *et al.*[17] (a) $5^1\Sigma^+$; (b) $2^1\Pi$; (c) $4^3\Sigma^+$; (d) $2^3\Pi$.

The total CT cross sections for Na(3p) are comparable in magnitude to those for Na(3s). It should be noted, however, that the final products and population distributions are quite different in the two cases. For the $He^+ + Na(3s)$ collision system, the cross section for the formation of He(1s2s) is larger by about an order of magnitude than that for He(1s2p). In contrast, for the $He^+ + Na(3p)$ system, the situation is reversed, with the He(1s2p) channel becoming the dominant electron-capture product. This difference can be understood in terms of the molecular-state couplings involved in the two collision systems. In the $He^+ + Na(3s)$ case, the dominant capture channel leading to He(1s2s) is nearly resonant with the entrance channel, which enhances the corresponding transition probability. However, when the initial state of sodium is Na(3p), the additional Π-type molecular symmetries and the associated nonadiabatic couplings favor transitions leading to the He(1s2p) state. As a result, the population of the He(1s2p) channel becomes significantly larger than that of He(1s2s) in the Na(3p) collision system.

By summing the state-resolved cross sections of the He^+–Na(3p) system in the singlet and triplet manifolds, the total CT cross sections for Na(3p) in the Σ and Π states are obtained, as shown in Fig. 11, and compared with previous results. For consistency with the literature, the notations Na($3p_{\|}$) and Na($3p_{\perp}$) are adopted in the present work, which correspond to the Σ and Π molecular states of the He^+–Na(3p) system, respectively. As shown in this figure, the CT cross sections originating from the Σ state are larger than those from the Π

state over the entire collision-energy range considered. This behavior indicates that the charge-transfer process is more efficient when the Na(3p) electron is aligned parallel to the internuclear axis. The difference between the two symmetries can be attributed to the distinct molecular couplings and interaction potentials associated with the Σ and Π states during the collision process. Consequently, the Σ-symmetry channels play a dominant role in the overall charge-transfer dynamics of the He^+–Na(3p) system.

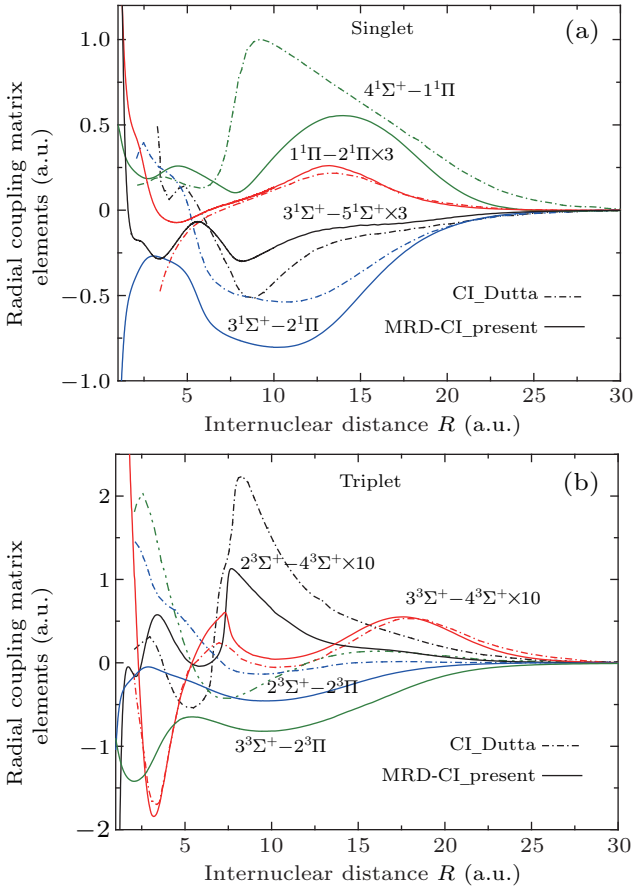


Fig. 10. Comparison of coupling matrix elements of $HeNa^+$ molecular states between the present MRD-CI method and CI of Dutta *et al.*[17] in the singlet (a) and triplet (b) spin manifolds.

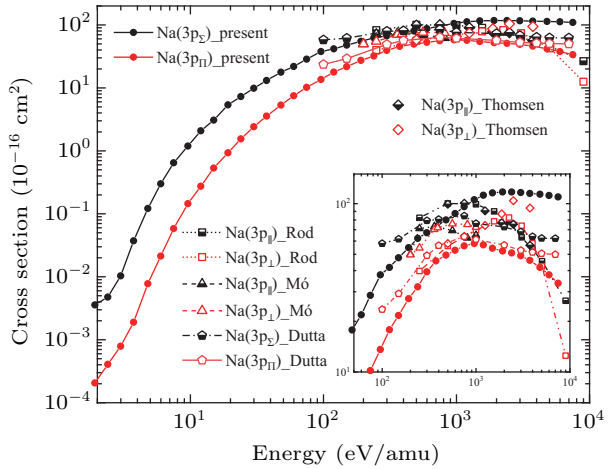


Fig. 11. Total QMOCC cross sections for charge transfer from Na(3p) in Σ and Π states, compared with previous results.

6. Conclusions

The adiabatic potential curves of the $HeNa^+$ system exhibit smooth long-range behavior dominated by polarization interactions, with pronounced avoided crossings appearing only at short internuclear distances. The associated radial and rotational couplings indicate that low-energy charge transfer is governed mainly by broad, long-range Demkov-type interactions, while short-range interactions become increasingly relevant at higher collision energies. These coupling features provide a clear understanding of the pathways and mechanisms controlling charge transfer in He^+–Na collisions.

For He^+–Na(3s) collisions, the total charge-transfer cross sections are dominated by the He(1s2s) triplet exit channel, consistent with quasi-resonant long-range interactions between entrance and exit channels. Excitation processes, occurring at shorter internuclear distances, are generally smaller in magnitude and involve more complex multichannel couplings. Oscillatory structures observed in the cross sections are attributed to Stueckelberg-type interference between successive avoided crossings, highlighting the coherent nature of charge-transfer dynamics.

For He^+–Na(3p) collisions, the presence of additional Π-symmetry channels significantly modifies the capture dynamics, leading to dominant population of the He(1s2p) state. Despite the different initial electronic configurations, the total charge-transfer cross sections remain comparable in magnitude to those for Na(3s), with Σ-symmetry channels contributing more efficiently than Π channels. Overall, the present QMOCC calculations provide a comprehensive and quantum-mechanically consistent description of low- and intermediate-energy collision dynamics in the He^+–Na system, in good agreement with available experimental and theoretical data.

Acknowledgment

Project supported by the National Natural Science Foundation of China (Grant Nos. 11774344, 12204288, and 12504293).

References

[1] Janev R K 1995 *Atomic and Molecular Processes in Fusion Edge Plasmas* (New York: Springer) pp. 225–280
[2] Fritsch W and Lin C D 1991 *Phys. Rep.* **202** 1
[3] Bransden B H and McDowell M R C 1992 *Charge Exchange and the Theory of Ion-Atom Collision* (Oxford: Clarendon Press) pp. 300–301
[4] Sidis V, Kubach C and Pommier J 1981 *Phys. Rev. A* **23** 119
[5] Mó O and Riera A 1988 *J. Phys. B: At. Mol. Opt. Phys.* **21** 119
[6] Fritsch W, Kimura M and Lane N F 1990 *Phys. Rev. A* **41** 508
[7] Wang X X, Wang K, Peng Y G, Liu C H, Liu L, Wu Y, Liebermann H P, Buenker R J and Qu Y Z 2021 *Chin. Phys. Lett.* **38** 113401
[8] Fan Y X, Xing D D, Cui S C, Wang X X, Ran J X, Lin K Z, Zhu X B, Zhao D M, Guo D L, Gao Y, Zhang S F, Zhu X L and Ma X W 2025 *Chin. Phys. B* **34** 073402
[9] Nielsen S E and Rod T H 1997 *J. Phys. B: At. Mol. Opt. Phys.* **30** 3833

[10] Nagata T, Okamura Y, Katoh E and Mukoyama Y 1981 *Phys. Lett. A* **81** 265
[11] DuBois R D and Toburen L H 1985 *Phys. Rev. A* **31** 3603
[12] Aumayr F, Lakits G and Winter H 1987 *Zeitschrift für Physik D* **6** 145
[13] Houver J C, Dowek D, Pommier J and Richter C 1989 *J. Phys. B: At. Mol. Opt. Phys.* **22** L585
[14] Thomsen J W, Andersen N, Dowek D, Houver J C, Larsson M O, Lauritsen J H V, Muller U, Pedersen J O P, Salgado J and Svensson A 1995 *J. Phys. B: At. Mol. Opt. Phys.* **28** L93
[15] Rod T H and Nielsen S E 1995 *J. Phys. B: At. Mol. Opt. Phys.* **28** L607
[16] Mó O and Riera A 1990 *J. Phys. B: At. Mol. Opt. Phys.* **23** L373
[17] Dutta C M, Lane N F and Kimura M 1994 *Phys. Rev. A* **49** 1806
[18] Kimura M and Lane N F 1989 *Adv. At. Mol. Opt. Phys.* **26** 79
[19] Wang J G, He B, Ning Y, Liu C L, Yan J, Stancil P C and Schultz D R 2006 *Phys. Rev. A* **74** 052709
[20] Zygelman B, Cooper D L, Ford M J, Dalgarno A, Gerratt J and Raimondi M 1992 *Phys. Rev. A* **46** 3846
[21] Buenker R J and Phillips R A 1985 *J. Mol. Struct.: Theochem* **123** 291
[22] Krebs S and Buenker R J 1995 *J. Chem. Phys.* **103** 5613
[23] Wang K, Qu Y Z, Liu C H, Liu L, Wu Y, Liebermann H P and Buenker R J 2020 *Chin. Phys. B* **29** 093401
[24] Lischka H, Nachtigallova D, Aquino A l J A, Szalay P t G, Plasser F, Machado F B C and Barbatti M 2018 *Chem. Rev.* **118** 7293
[25] Dunning T H 1989 *J. Chem. Phys.* **90** 1007
[26] Fernandez Pacios L and Christiansen P A 1985 *J. Chem. Phys.* **82** 2664
[27] Kramida A, Ralchenko Y, Reader J and NIST ASD Team 2019 *NIST Atomic Spectra Database* (National Institute of Standards and Technology, Gaithersburg, MD.)
[28] Herrero B, Cooper I L and Dickinson A S 1996 *J. Phys. B: At. Mol. Opt. Phys.* **29** 5583
[29] Heil T G, Butler S E and Dalgarno A 1981 *Phys. Rev. A* **23** 1100
[30] Abramowitz M and Stegun I A 1970 *Handbook of Mathematical Functions* (Dover)
[31] Liu C H, Liu L, Qu Y Z, Wang J G and Janev R K 2010 *Phys. Rev. A* **82** 022710
[32] Johnson B R 1973 *J. Comput. Phys.* **13** 445
[33] Gargaud M, Mccarroll R and Valiron P 1987 *J. Phys. B: At. Mol. Phys.* **20** 1555
[34] Kimura M and Lane N F 1990 *Phys. Rev. A* **41** 5938
[35] Liu C H and Wang J G 2017 *Eur. Phys. J. D* **71** 168